

Coexistence of Self-Organized Criticality and Intermittent Turbulence in the Solar Corona

Vadim M. Uritsky,^{1,*} Maya Paczuski,¹ Joseph M. Davila,² and Shaela I. Jones³

¹*Complexity Science Group, Department of Physics and Astronomy,
University of Calgary, Calgary, Alberta, Canada T2N 1N4*

²*NASA Goddard Space Flight Center, Greenbelt, MD 20771, USA*

³*University of Maryland, College Park, MD 20742, USA*

(Dated: December 2, 2024)

An extended data set of extreme ultraviolet images of the solar corona provided by the SOHO spacecraft are analyzed using statistical methods common to studies of self-organized criticality (SOC) and to intermittent turbulence. The data exhibits simultaneous hallmarks of both regimes, namely power-law avalanche statistics as well as multiscaling of structure functions of spatial activity. This indicates that both SOC and intermittent turbulence may be manifestations of a single dynamical process in magnetized plasmas entangling avalanches of magnetic energy dissipation with turbulent particle flows.

PACS numbers: 05.65+b, 52.35.Ra, 96.60.qe

Intermittent turbulence and SOC represent two paths to dynamical complexity in driven, extended nonlinear systems. Some authors have argued that they are distinct, unrelated phenomena [1, 2, 3, 4], while others have suggested a fundamental connection [5, 6, 7, 8, 9, 10]. The problem is rooted in the fact that both paths produce scaling patterns from seemingly different microscopic rules. In classical fluid turbulence, scaling is associated with a hierarchical structure of eddies extending over the inertial range [11]. In SOC, avalanches of localized instabilities organize the system toward a steady state that exhibits long-range correlations up to the system size [12].

For some years, Bak and co-workers have speculated that turbulence in the limit of high Reynolds number (HRN) may be a SOC phenomenon [5, 13, 14, 15]. It has been suggested [5, 7, 9] that dynamical transitions observed in HRN turbulence are critical avalanches of dissipation. However, the primary source of energy in fluid turbulence is kinetic, while SOC is driven by instabilities in potential energy stored in the medium at least according to the models developed so far. The two forms of energy could coexist in magnetized plasmas with current-dependent resistivity switching the plasma between states dominated by convection to states with rapid diffusion of magnetic field lines [16]. In the plasma frame, this process resembles stick-slip or depinning transitions of SOC models [17, 18, 19], and produces scale-free energy dissipation suggestive of SOC in models of magnetized plasmas [16, 20, 21]. It is also analogous to rice pile dynamics [22], where kinetic energy of grains releases stored potential (gravitational) energy.

In order to clarify this issue, we present direct observational evidence for coexistence of SOC and intermittent turbulence in the magnetized plasma of the solar corona. Using a single high resolution data set, we apply two different analysis methods – one (SOC method) for analyzing

avalanche statistics of the emission field and the other (turbulence method) for analyzing structure functions of the same field. The energy, area and lifetime statistics of avalanches detected in this data set obey robust scaling laws. Unlike previous studies of flare statistics, we use a spatiotemporal event detection algorithm compatible with the usual definition of avalanches in SOC. Next, we show that the same data set exhibits multiscaling and extended self-similarity (ESS) of higher order structure functions – a hallmark of intermittent turbulent phenomena. The observed scaling behaviors show only weak dependence on average solar activity and were found both at solar minimum (min) and maximum (max), indicating that coexistence of SOC and intermittent turbulence is a generic characteristic of coronal behavior.

Dissipation mechanisms in the corona are activated by changes in the configuration of the coronal magnetic field. Convection of magnetic fields leads to radiative transients, plasma jets, and explosive events known as solar flares [23, 24, 25]. The latter are associated with intense and spatially concentrated release of magnetic energy accompanied by localized plasma heating up to temperatures of 10^7K , and can be observed by short-wavelength light emission. Flares tend to appear at irregular times and locations and exhibit broadband energy, size and lifetime statistics with no obvious characteristics scales. This behavior is often interpreted as a signature of SOC [24, 26, 27, 28, 29, 30, 31]. Further, the configuration of magnetic flux in the corona has been shown empirically to form a scale-free network with statistical features that can be captured with a simple model [31, 32]. The magnetic field inside active coronal regions also has an intermittent spatial structure which reorganizes during large flares [10, 33, 34]. The results of our study suggest, though, that the connection between SOC and turbulence is a generic phenomenon not limited to large flares.

We have studied time series of full-disk digital images of the corona taken by the extreme ultraviolet imaging telescope (EIT) onboard the SOHO spacecraft [25, 35] in the 195 Å wavelength band corresponding to the Fe XII emission at peak coronal temperatures of $1.6 \cdot 10^6$ K [25]. The redistribution of brightness seen in consecutive EIT frames reflects processes of energy transport and release due to the emergence and evolution of specific coronal features such as loops and holes, mass ejections, and other phenomena. The data included two observation periods: 06/29/2001 - 07/28/2001 (3240 images, solar max, average sunspot number 64.0) and 10/22/2005 - 12/02/2005 (4407 images, solar min, average sunspot number 16.3) with a typical time resolution of 13.3 min. To avoid optical distortions at the edges of the Sun disk, we studied only its central portion with the linear dimensions 1040×1040 Mm (256×256 pixels with 5.6 arcsec spatial resolution). The EIT luminosity $w(t, \mathbf{r})$ was analyzed as a function of time t and position \mathbf{r} on the image plane. For the purpose of this study, we treated $w(t, \mathbf{r})$ as a local measure of coronal activity. Therefore, we did not filter the data in an attempt to distinguish between different types of coronal events. Our analysis was based on two alternative approaches allowing a study of $w(t, \mathbf{r})$ both as an impulsive avalanching process and a continuum turbulent field – as shown in Fig. 1.

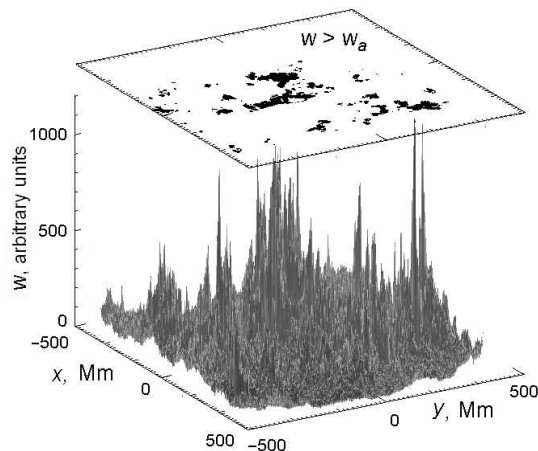


FIG. 1: Two views of the solar corona's complexity. Upper panel: snapshots of high activity coronal regions used to construct avalanches ($w_a = 350$). Lower panel: a snapshot of the continuous brightness field at the same time instant.

To identify avalanches, we used a spatiotemporal detection method [36] that resolves concurrent events. First, avalanching regions were identified by applying an activity threshold w_a representing a background EUV flux. Contiguous spatial regions with $w(\mathbf{r}, t) > w_a$ were treated as pieces of evolving avalanches. By checking for overlap of common pixels between each pair of consecutive EIT frames, we identified a set of 3-dimensional

spatiotemporal integration domains $\Lambda_i (i = 1, \dots, N)$ corresponding to each of N individual avalanches. These domains of contiguous activity in space and time were used to compute the lifetimes, $T_i = \max(t \in \Lambda_i) - \min(t \in \Lambda_i)$, the radiative emission flux, $E_i = \int_{\Lambda_i} w(\mathbf{r}, t) d\mathbf{r} dt$, as well as the peak areas, $A_i = \max_t (\int_{\Lambda_i(t)} d\mathbf{r})$, or maximum number of pixels in a snapshot of each avalanche. Active regions that split after starting at a unique source were considered parts of a single avalanche. Active regions that merged were considered as separate avalanches, with the common "tail" ascribed to the event that started earlier. Only events that lasted at least two successive time frames and were not truncated by the field of view or temporal gaps in observations longer than 40 min were selected for subsequent analysis. The robustness of the obtained statistics was verified by repeatedly running the algorithm with substantially different w_a . Due to large difference in average emission, $\langle w \rangle$, during solar min and max, w_a were defined relative to $\langle w \rangle$ for each data set. Depending on w_a , between 4,830 (1,680) and 26,900 (5,350) coronal events were detected for solar max (min).

Fig. 2 shows probability distributions for avalanche lifetime, total emission flux and peak area for both solar max and min. These statistics can be approximately fitted by the power-law relations $p(T) \sim T^{-\tau_T}$, $p(E) \sim E^{-\tau_E}$ and $p(A) \sim A^{-\tau_A}$ with the exponents being almost independent of w_a . The same exponents have also been found using a fluctuating threshold placed at 3 standard deviations above the average brightness of each image. The large-scale rollovers are due to the absence of events whose lifetimes are comparable to or larger than the maximum available time scale $5.2 \cdot 10^5$ s given by the ratio between the latitudinal size of the field of view and the rotation velocity at the solar equator. Such events tend to cross the field of view and are therefore underrepresented in our sample.

The exponents observed at solar max ($\tau_T = 2.02 \pm 0.05$, $\tau_E = 1.70 \pm 0.04$, $\tau_A = 2.53 \pm 0.09$) and at solar min ($\tau_T = 1.96 \pm 0.06$, $\tau_E = 1.66 \pm 0.03$, $\tau_A = 2.51 \pm 0.14$) are indistinguishable within uncertainties. This is also true for the exponents z , D_E and D_A defined by the relations $T \sim l^z$, $E \sim l^{D_E}$ and $A \sim l^{D_A}$, where l is the linear avalanche scale [49]. The resulting values are $z = 1.94 \pm 0.12$, $D_E = 3.16 \pm 0.21$ and $D_A = 1.50 \pm 0.10$ for solar max and $z = 2.09 \pm 0.17$, $D_E = 3.34 \pm 0.25$ and $D_A = 1.50 \pm 0.10$ for solar min. All values were obtained by averaging over four activity thresholds ($w_a = k \langle w \rangle$, where $k \in \{0.4, 0.8, 1.2, 1.6\}$) within fixed ranges of emission flux, time and space scales corresponding to the power-law portions of the relations. The reported uncertainties are the standard errors from this averaging or from the regression estimate at individual thresholds, whichever is larger. Up to these errors, the exponents satisfy the conservation relations $z(\tau_T - 1) = D_E(\tau_E - 1) = D_A(\tau_A - 1)$ predicted for SOC.

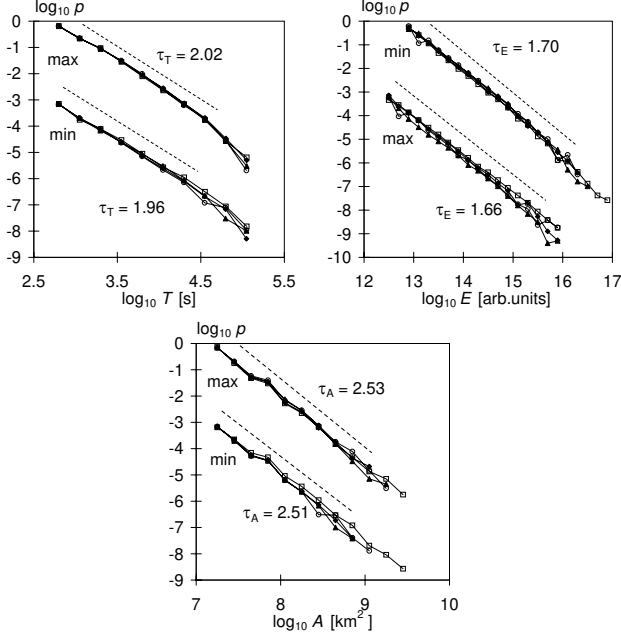


FIG. 2: Probability distributions of avalanche lifetime, emission flux and peak area for solar max and min at four different thresholds $w_a = k \langle w \rangle$ with $k = 0.4$ (squares), $k=0.8$ (diamonds), $k=1.2$ (triangles) and $k=1.6$ (circles). The min distributions are shifted downward for comparison.

All these results support the hypothesis that the corona operates in a SOC state. Qualitatively our findings agree with earlier works on solar flare statistics (see e.g. [26, 27, 28]). The exponent τ_T is consistent with previous analyses of threshold-dependent inter-occurrence times of x-ray bursts measured over the whole Sun [37], as would be expected if total emission were a sum over individual avalanches [38]. Its value as well as $z \approx 2$ indicate that the corona may operate at a mean-field limit [39]. The other exponents are new and cannot be compared with previous works where single events were not resolved – except for a few case studies [24, 29] focusing on specific coronal conditions.

We have also analyzed coronal activity as a continuum turbulent field. Such analyses are normally accomplished by measuring a set of structure functions for the relevant dynamical variable δz represented by longitudinal increments of the velocity field \mathbf{v} [11] or, in the case of MHD turbulence, of the Elsässer variables $\mathbf{v} \pm \mathbf{B}$, where \mathbf{B} is the magnetic field [40, 41]. Taking δz proportional to differences in the scalar field $w(\mathbf{r}, t)$ measured by SOHO EIT, we define the structure functions to be

$$S_q(l) = \langle |w(\mathbf{r}, t) - w(\mathbf{r} + \delta\mathbf{r}, t)|^q \rangle_{\mathbf{r}} \quad (1)$$

Here q is the order of the structure function, $\delta\mathbf{r}$ is the spatial displacement, $l \equiv |\delta\mathbf{r}|$, and averaging indicated by brackets is performed over all positions \mathbf{r} . Within the inertial range, $S_q(l) \sim l^{\zeta(q)}$ with $\zeta(q)$ defined by the

turbulent regime under study. In practice, scaling directly in $S_q(l)$ can be extremely limited. This is exactly the issue we faced when analyzing the coronal images (Fig. 3). The behavior is approximately isotropic (see the inset in Fig. 4) and so could not be eliminated by projecting the data on the irreducible representations of the $SO(2)$ symmetry group [42]. In such situations, the ESS method [43] is often used [50]. ESS tends to extend the observed range of scaling making it possible to estimate relative exponents.

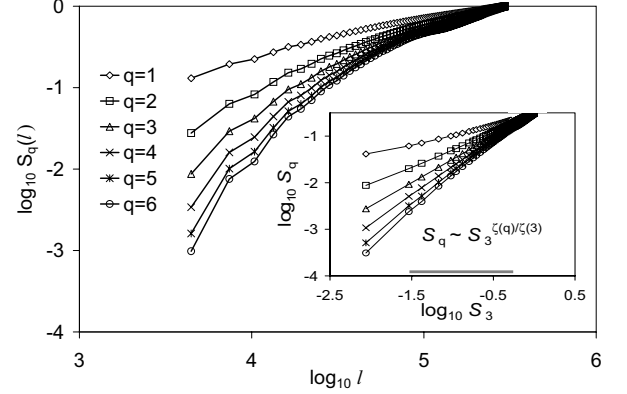


FIG. 3: Structure functions of coronal activity. Each function is normalized by its maximum value. Inset: ESS scaling of the structure functions. The horizontal bar indicates the range used for estimating exponents.

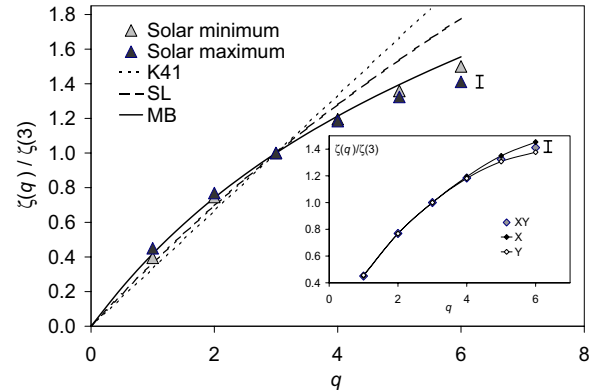


FIG. 4: ESS exponents as compared to the Kolmogorov $q/3$ scaling (K41) and hierarchical models of intermittent turbulence defined in the text. Inset: solar maximum exponents obtained for horizontal (X), vertical (Y), and arbitrary (XY) orientations of the displacement vector $\delta\mathbf{r}$, as a test for isotropy. Vertical error bars show the discrepancy between horizontal and vertical $\zeta(6)$ estimates at solar max.

The functions $S_q(l)$ exhibit ESS over almost the entire range (Fig. 3, inset). The dependence of the relative ESS exponent $\zeta(q)/\zeta(3)$ on the order q (Fig. 4) shows a clear departure from the Kolmogorov law. To clarify the origin of this intermittency, we have tested several analytical fits

encompassed by a hierarchical model [44, 45]:

$$\zeta(q) = (q/g)(1-x) + C(1 - (1-x/C)^{q/g}) \quad (2)$$

The model contains three tuning parameters defined by the relations $\delta z \sim \ell^{1/g}$, $t_e \sim \ell^x$, and $C = 3 - D$, where t_e is the energy transfer time at smallest inertial scales ℓ and D is the dimension of the dissipative structures. The She-Leveque (SL) model [46] with vortex filaments ($D = 1$) is obtained substituting $g = 3$, $x = 2/3$, and $C = 2$. The Iroshnikov-Kraichnana MHD model [40] assumes $g = 4$, $x = 1/2$, and $C = 1$ with dissipative structures interpreted as current sheets and predicts values of the relative exponents which for the q range considered here are indistinguishable from the SL model. The combination $g = 3$, $x = 2/3$, and $C = 1$ gives the Müller-Biskamp (MB) model [45] implying that turbulence occurs in a 3d MHD system with basic hydrodynamic scaling and sheet-like dissipative structures. As Fig. 4 shows, the latter provides the best overall description for our data. Note that the error bar shown in the figure is the uncertainty coming from the slight anisotropy shown in the inset.

Our main finding is the simultaneous appearance of robust signatures of both SOC and intermittent turbulence in a single time series of coronal images including significantly different phases of the solar cycle. These observations can be interpreted using two physical scenarios. The first one assumes that turbulence in coronal dissipation is passively driven by SOC avalanches of dissipating coronal currents which can modify the coronal magnetic field [10, 33]. The second scenario implies a more collaborative connection between SOC and MHD turbulence in which SOC avalanches of reconnecting magnetic loops [26, 30, 31] generate inward and outward plasma flows [47] and/or cascades of MHD shock waves [48] working as sources of localized turbulence and turbulence-driven anomalous resistivity regions for new reconnections sites. Testing these scenarios requires further analysis of spatiotemporal patterns of the coronal magnetic field.

The mechanisms we discuss are basic and can appear in various types of driven magnetized plasmas. As a result, coexistence of SOC and intermittent turbulence may be a generic feature of spatiotemporal complexity in many astrophysical situations.

* Also at the Saint Petersburg University, Russia; Electronic address: vuritsky@phas.ualgary.ca

- [1] G. Boffetta et al., Phys. Rev. Lett. **83**, 4662 (2001).
- [2] V. Antoni et al., Phys. Rev. Lett. **87**, 045001 (2001).
- [3] V. Carbone et al., Europhys. Lett. **58**, 349 (2002).
- [4] E. Spada et al., Phys. Rev. Lett. **86**, 3032 (2001).
- [5] P. Bak and M. Paczuski, Physica A **348**, 277 (2005).
- [6] K. Chen and C. Jayaprakash, Physica A **340**, 566 (2004).
- [7] K. R. Sreenivasan et al., Physica A **340**, 574 (2004).
- [8] T. Chang, Phys. Plasmas **6**, 4137 (1999).
- [9] M. Paczuski et al., Phys. Rev. Lett. **95**, 181102 (2005).
- [10] V. I. Abramenko and V. B. Yurchyshyn, Astrophys. J. **597**, 1135 (2003).
- [11] A. Kolmogorov, Dokl. Akad. Nauk SSSR **31**, 538 (1941).
- [12] P. Bak et al., Phys. Rev. Lett. **59**, 381 (1987).
- [13] P. Bak et al., Phys. Lett. A **147**, 297 (1990).
- [14] K. Chen et al., Physica A **340**, 566 (2003).
- [15] M. Paczuski and P. Bak, Phys. Rev. E **48**, R3214 (1993).
- [16] A. J. Klimas et al., J. Geophys. Res.-Space Physics **105**, 18765 (2000).
- [17] P. Bak and C. Tang, J. Geoph. Res.-Solid Earth and Planets **94**, 15635 (1989).
- [18] Z. Olami et al., Phys. Rev. Lett. **68**, 1244 (1992).
- [19] M. Paczuski et al., Phys. Rev. E **53**, 414 (1996).
- [20] V. M. Uritsky et al., Phys. Rev. E **65**, 046113 (2002).
- [21] A. J. Klimas et al., J. Geophys. Res.-Space Physics **109**, 1426 (2004).
- [22] V. Frette et al., Nature **379**, 49 (1996).
- [23] M. J. Aschwanden, *Physics of the Solar Corona* (Springer, 2005).
- [24] D. Berghmans and F. Clette, Sol. Phys. **186**, 207 (1999).
- [25] J.-P. Delaboudiniere et al., Sol. Phys. **162**, 291 (1995).
- [26] P. Charbonneau et al., Sol. Phys. **203**, 321 (2001).
- [27] M. J. Aschwanden and C. E. Parnell, Astrophys. J. **572**, 1048 (2002).
- [28] C. E. Parnell and P. E. Jupp, Astrophys. J. **529**, 554 (2000).
- [29] D. Berghmans et al., Astron. Astrophys. **336**, 1039 (1998).
- [30] E. T. Lu and R. J. Hamilton, Astrophys. J. **380**, L89 (1991).
- [31] D. Hughes et al., Phys. Rev. Lett. **90**, 131101 (2003).
- [32] D. Hughes et al., Physica A **34**, 158 (2004).
- [33] V. I. Abramenko et al., Astrophys. J. **577**, 487 (2002).
- [34] L. Sorriso-Valvo et al., Planetary Space Sci. **52**, 937 (2004).
- [35] <http://umbra.nascom.nasa.gov/eit/>.
- [36] V. M. Uritsky et al., J. Geophys. Res.-Space Physics **107**, 1426 (2002).
- [37] M. Baiesi et al., Phys. Rev. Lett. **96**, 051103 (2006).
- [38] A. Corral and M. Paczuski, Phys. Rev. Lett. **83**, 572 (1999).
- [39] C. Tang and P. Bak, J. Stat. Phys. **51**, 797 (1988).
- [40] P. S. Iroshnikov, Sov. Astron. Zh. **40**, 742 (1963).
- [41] R. H. Kraichnan, Phys. Fluids **8**, 1385 (1965).
- [42] E. Bouchbinder et al., Phys. Rev. Lett. **95**, 255503 (2005).
- [43] R. Benzi et al., Phys. Rev. E **48**, R29 (1993).
- [44] Z.-S. She and E. C. Waymire, Phys. Rev. Lett. **74**, 262 (1995).
- [45] W.-C. Muller and D. Biskamp, Phys. Rev. Lett. **84**, 475 (2000).
- [46] Z.-S. She and E. Leveque, Phys. Rev. Lett. **72**, 336 (1994).
- [47] N. Narukage and K. Shibata, Astrophys. J. **637**, 1122 (2006).
- [48] M. Ryutova and T. Tarbell, Phys. Rev. Lett. **90**, 191101 (2003).
- [49] The exponent D_A was estimated by counting the number N_A of non-overlapping boxes of size l needed to cover the active region at the peak of the avalanche, using $N_A(l) \sim l^{-D_A}$. The exponents z and D_A were obtained from regression plots $T(A)$ and $E(A)$ assuming $A \sim l^{D_A}$.

[50] This is usually done by plotting $S_q(l)$ versus $S_3(l)$